Phase Correction and DNN Heartbeat Estimation for Vital Signs Monitoring using FMCW Radar

Shihao Zhang, Zhaozong Meng, Yongwei Zhang, Murat Temiz, Orhan Kaplan, Nan Gao, Zonghua Zhang

***Abstract*—Due to its multi-objective potential for noncontact vital signs monitoring, millimeter-wave (mmW) radar has increasingly drawn attention in human health and safety related sensing applications. However, detection of vital signs, especially weak heartbeat reaction, is more challenging when disrupted by interference from background noise, random human body movement, and sensitive nature of radio waves. To address these problems, the work presents an improved Frequency Modulated Continuous Wave (FMCW) radar vital signs monitoring solution incorporating phase error correction and heartbeat event probability prediction. The main contributions include: (1) Development of a data processing framework reinforcing radar echoes for high Signal-to-Noise Ratio (SNR) vital signs detection, which amplified the returned signals through beamforming, and compensated phase perturbation. Additionally, two techniques including adaptive mode decomposition and neural network have been cordially adopted to perform signal conditioning; (2) Proposal of a phase error correction method with an adaptive dual-sliding window to mitigate the phase noise and distortion introduced by the non-periodic body movement, non-stationary breathing pattern, and dynamic environmental clutter, etc. It overcomes susceptibility to noise for the phase response and improves its stability and continuity; (3) Establishment of a Deep Neural Network (DNN)-based model to predict the probability distribution of heartbeat events with phase segmentation. This prediction model avoids rigid misclassification of heartbeats, and enhances the algorithm's tolerance to noise and adaptability to complex conditions. Experimental results have verified the effectiveness of the proposed solutions. The presented method provides a robust solution for reliable, high accuracy, and continuous vital signs monitoring in real environments.**

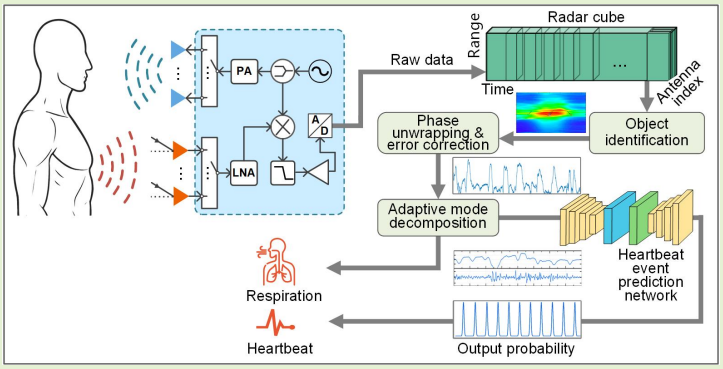

***Index Terms*—FMCW radar, vital signs monitoring, beamforming, phase error correction, DNN heartbeat estimation**

I. Introduction

Vital signs monitoring is indispensable in diverse human health and safety-related applications, including medical care, remote health monitoring, driver status monitoring, underground work sensing, and post-disaster search and rescue. Many contact sensing solutions, such as Electrocardiography (ECG) and Photoplethysmography (PPG), will inevitably introduce constraints to individuals' daily activities [1,2], which also limit their applications to in-hospital medical treatment. Non-contact sensing technologies that are free of restrictions on human activities are more competitive in satisfying the requirements of different application scenarios. However, novel non-contact measurement approaches, such as vision-based techniques and optical vibrocardiography [3], are susceptible to ambient lighting conditions and may raise risks of privacy leakage [3,4]. Frequency Modulated Continuous Wave (FMCW) millimeter-wave radar technology, for its high-resolution ranging and short-wavelength phase sensitivity, demonstrates great potential in detecting subtle physiological movements caused by respiration and heartbeat. Although FMCW radar vital signs detection has gained research effort and significant progress has been made in recent years, it still faces some key challenges including interference from human micro-movements such as subtle body posture changes and limb movements, overlapping of weak heartbeat signal with harmonics of respiration signal, clutter caused by the movement of ambient people or objects, and the inherent sensitive property of radar phase signal.

To address the above challenges, this investigation proposes a phase error correction and heartbeat event probability

This work was supported in part by the National Natural Science Foundation of China (NSFC) under Grants 62361136811, the Natural Science Foundation of Hebei Province under Grant E2022202128, TUBITAK Grant 123N800, and METUBAP Grant AGEP-301-2025-11558. (Corresponding authors: Zhaozong Meng and Yongwei Zhang, Emails: zhaozong.meng@hebut.edu.cn, David.y.zhang@ntu.edu.cn)

Shihao Zhang, Zhaozong Meng, Nan Gao, and Zonghua Zhang are with School of Mechanical Engineering, Hebei University of Technology, Tianjin 300401, China. (Email: zhi56211@outlook.com)

David Zhang is with School of Transportation and Civil Engineering, Nantong University, Nantong 226019, China.

Murat Temiz is with Middle East Technical University, Ankara, Türkiye, and also with University College London, London, UK.

Orhan Kaplan is with Faculty of Technology, Gazi University, Ankara 06570, Türkiye.

prediction enhanced FMCW radar vital signs monitoring technique. The objective is to enhance and extract weak vital signs affected by human micro-motions and complex environmental factors. The main contributions of this investigation include:

(1) A framework for the enhancement and high Signal-to-Noise Ratio (SNR) extraction of radar vital sign signals is proposed. This framework integrates pre-processing methods, including object identification, beamforming signal reinforcement, and phase signal correction. Adaptive vital signs modal decomposition is utilized to obtain distinct vital sign modes, and subsequently, the heartbeat signal component is input into a deep neural network to predict a sequence of heartbeat event probabilities to obtain robust vital signs.

(2) An adaptive dual-sliding window phase error correction method is proposed to deal with the susceptibility of FMCW radar phase signals to various complex interference factors, and to effectively suppress phase noise and distortion introduced by target aperiodic micro-motions, non-stationary respiratory patterns, dynamic environmental clutter, and potential electromagnetic interference. This method can effectively enhance the stability and continuity of the radar phase signal, which is important for the subsequent signal analysis.

(3) A Deep Neural Network (DNN) model for heartbeat event probability prediction with weak and noisy heartbeat signals is developed for heartbeat detection. To create a more effective reference signal for the network, the discrete sequence of heartbeat events is converted into a sequence of Gaussian probability distributions centered by the heartbeat events. This model predicts the probability distribution of heartbeat events with a longer radar phase segment instead of directly regressing the heartbeat or performing binary classification of heartbeat events. This approach effectively handles occasional probability deviations caused by interference, thereby improving the algorithm's noise tolerance and enhancing its adaptability to practical and complex environmental influences.

By employing the presented techniques, including signal reinforcement and extraction framework, adaptive phase error correction, and heartbeat event probability prediction model, this investigation offers an effective solution to handle the key challenges facing this area.

This study focuses on improving the performance of continuous heartbeat detection of a single specified individual using 60 GHz FMCW radar in the presence of signal interference in a typical application environment. The remainder of this paper is organized as follows: Section II summarizes related work of radar-based vital signs detection and gives an analysis of existing applications, algorithms, and potential challenges. Section III elaborates on the proposed signal processing framework and the proposed technical solutions. Section IV presents the experimental verification and results analysis to validate the effectiveness of the proposed methods. Finally, Section V concludes the work and envisages the future.

II. Related Work

This section surveys the related research on radar-based vital signs detection. It begins with outlining the emerging applications, then discusses the key processing algorithms, subsequently analyzes the challenges facing current research, and finally, gives the objectives of this investigation.

A. Emerging Applications of Radar Vital Signs Sensing

Currently, the four mainstream radar technologies used for vital signs monitoring are Continuous Wave (CW) [5,6], Frequency Modulated Continuous Wave (FMCW) [7-9], Ultra-Wideband (UWB) [10,11], and Stepped-Frequency Continuous Wave (SFCW) [12,13]. CW radar features high sensitivity and simple architecture [14,15] but lacks modulation information, rendering it incapable of distance measurement. UWB radar offers a high SNR. However, its ultra-wideband nature results in a complex hardware structure [16,17]. FMCW radar gives rich measurement information through frequency modulation and is characterized by high integration, low power consumption, and relatively high range resolution. A recent comprehensive comparison further validates that although both CW and FMCW configurations can measure respiration and heart rates, FMCW offers superior performance in identifying specific cardiac events and extracting advanced biomarkers like Heart Rate Variability (HRV) [18]. FMCW radars operating in the millimeter-wave band are currently more commonly used, with related technological advancements and innovative applications being continuously reported, as summarized in recent surveys [19].

Millimeter-wave radar, due to its technical advantages in sensing applications, has demonstrated extensive application prospects in the field of non-contact vital signs monitoring. In healthcare, radar systems are employed for continuous vital signs monitoring of seriously ill patients, which could reduce the discomfort associated with contact sensors and lower the risk of cross-infection [20]. Concurrently, this technology is widely applied in home environments for remote health monitoring of the elderly or patients with chronic diseases. For instance, the use of FMCW radar for preliminary screening of respiratory patterns highlights its potential in convenient home healthcare [21]. The application scope has recently expanded to more complex scenarios and extended the boundaries of remote health assessment, such as rotary FMCW radar for omnidirectional, multi-person localization and simultaneous vital signs detection [22], and even non-contact multi-target HRV detection [23]. Furthermore, this technology is also gaining prominence in emerging fields such as post-disaster search and rescue, security, and human-computer interaction. In post-disaster scenarios, long-wavelength radar is used to penetrate obstacles to detect the vital signs of trapped individuals [24]. In smart homes, it can adjust home facilities settings by perceiving user physiological parameters. The diverse applications and their scenario complexity place higher demands on the continuity, accuracy, and robustness of vital signs monitoring.

B. Progress of Radar Data Signal Processing Algorithms

Radar data processing algorithms are pivotal in determining the reconstruction quality of vital sign signals. Addressing common technical challenges in radar vital signs

signal extraction, such as the susceptibility of weak heartbeat signals to human micro-motions, respiratory harmonics, and environmental interference, current research in data processing algorithms primarily focuses on developing more effective noise and interference suppression methods, accurate signal separation techniques, and the integration of intelligent algorithms like deep learning. The primary goal is to comprehensively enhance the accuracy, robustness, and real-time performance of vital signs monitoring.

To improve the effectiveness and robustness of algorithmic analysis, accurately separating various frequency components within the signal spectrum and strengthening the algorithm's anti-noise interference capabilities are crucial prerequisites. The Fast Fourier Transform (FFT), as a fundamental frequency-domain analysis tool, reveals the overall frequency composition of a signal. Wavelet transforms provide time-frequency localization capabilities. Specifically, the Continuous Wavelet Transform (CWT), through scaling and translating a mother wavelet, can effectively characterize the time-frequency properties of signals at different scales, which makes it particularly suitable for the analysis of non-stationary signals like vital signs [25]. Mode decomposition methods aim to decompose complex signals into several Intrinsic Mode Functions (IMFs) with specific physical meanings, thereby achieving effective separation of overlapping frequencies in the spectrum. Empirical Mode Decomposition (EMD) is an adaptive signal decomposition method, but it is sensitive to noise and suffers from issues like end effects and mode mixing [26]. To overcome these shortcomings of EMD, numerous improved methods have been developed. For example, the Empirical Wavelet Transform (EWT) combines the adaptivity of EMD with the theoretical framework of wavelet transforms by adaptively segmenting the signal's Fourier spectrum to construct suitable wavelet filter banks, thereby extracting more physically interpretable AM-FM components [27]. Another method receiving considerable attention is Variational Mode Decomposition (VMD), which introduces a variational model. Through a constrained iterative optimization process, VMD adaptively determines the center frequency and bandwidth of each mode, thus decomposing signals more robustly and balancing errors among the mode functions [28]. Considering the importance of parameter selection for VMD, recent work focused on adaptive optimization. For instance, the Health-VMD method utilizes an improved grasshopper optimization algorithm to adaptively select VMD parameters, enabling more accurate extraction of heartbeat waveforms for HRV analysis in multi-target scenarios [23]. A similar approach, Successive Variational Mode Decomposition (SVMD), was effectively applied to decompose and reconstruct breathing and heartbeat signals in noisy in-vehicle environments [29]. Additionally, other improved schemes such as the Zero-Attracting Sign Least Mean Square (ZA-SLMS) technique [30] and peak detection techniques [31,32] were employed for the suppression of strong motion and interference cancellation.

In addition, enhancing the robustness of radar sensing against body movements has been regarded as a recent research focus. To address this, strategies have been developed to compensate for both the subject's movement and the sensor's own movement. For subject movement, a hybrid signal model was established for vital signs detection in various body postures, with a periodic signal enhancement algorithm to isolate vital signs from limb motion interference [33]. For non-periodic body movements, an adaptive motion noise cancellation scheme based on virtual antenna arrays was proposed to suppress nonlinear noise [34]. Another innovative technique treated signal segments corrupted by RBM as missing data[35]. By identifying RBM periods, a missing data model was established, and compressed sensing was then used to accurately recover the vital signs from the incomplete data. Furthermore, to handle large-scale displacements where a target crossed multiple range bins, a phase compensation method was proposed to demodulate the baseband signal using the target's estimated distance, thereby enabling wide-range and accurate displacement measurement [36]. On the other hand, for the motion of the sensor itself, such as handheld applications, a novel multimodal sensing method was proposed [37], which utilized the built-in Inertial Measurement Unit (IMU) of the device to record and compensate for the motion artifacts caused by the device vibration, thereby achieving accurate vital sign measurement.

Moreover, deep learning techniques are increasingly being incorporated into the reconstruction of vital sign signals to enhance measurement accuracy. Mauro et al. utilized a Convolutional Variational Autoencoder (C-VAE) to correlate measured signals with reference signals, constructing a deep learning model and generalizing it to diverse subjects via meta-learning for respiratory signal reconstruction [38]. Wang et al. employed neural networks to identify heartbeat signal patterns, significantly improving the SNR of heartbeat signals and leveraging historical data to further enhance the accuracy of current heart rate estimation [39]. Numen et al. implemented a DNN for joint vital signs and occupancy classification, achieving high accuracy in four-category respiration-state classification based on frequency and occupancy status [40]. However, due to real-time application requirements and limitations of embedded computing platform resources, model effectiveness and computational lightweighting of deep learning networks are major concerns in this field.

C. Technical Challenges

Despite the significant progress in existing research, radar-based vital signs monitoring still faces several challenges in practical applications. Signal distortion and interference caused by human micro-motions, coupling between respiration and heartbeat, and environmental clutter interference remain common difficulties in this domain. Research into vital signs signal enhancement and high SNR signal extraction techniques to achieve accurate measurement of respiratory and heartbeat signals is of great importance for both research and practice.

Human micro-motions, such as slight postural adjustments or limb swings, generate motion artifact signals with amplitudes far exceeding those of the subtle physiological displacements caused by heartbeats. These artifacts can interfere with vital sign signals, potentially even completely overwhelming the useful signals. Harmonics of the respiratory signal may overlap with the fundamental frequency of the heartbeat signal, making the accurate separation and extraction of weak heartbeat signals from a strong respiratory background particularly challenging. Environmental clutter interference,

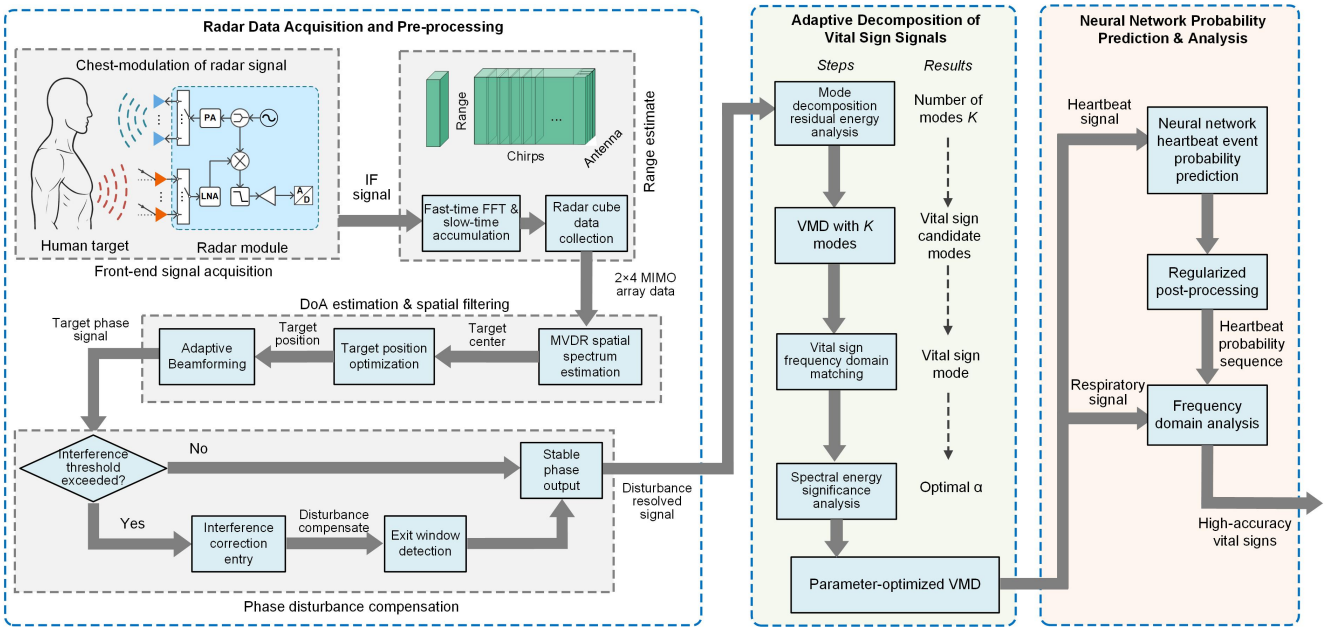

Fig. 1. The proposed framework for radar vital sign signals enhancement and high SNR extraction.

such as movements from nearby individuals and objects, introduces additional dynamic noise, further reducing the SNR of the target vital signs signal. Additionally, vital signs from other targets at similar distances can be mixed into the signal of the target of interest, thereby reducing the accuracy of vital signs extraction. Furthermore, disturbances to the signal caused by factors such as multipath effects and electromagnetic interference in the space can also affect signal quality. The severe attenuation of signal strength when short-wavelength electromagnetic waves penetrate obstacles like walls can lead to decreased environmental adaptability.

In real-world scenarios where multiple interference factors coexist, the continuous and reliable heartbeat monitoring for a specific individual remains a critical technical challenge that needs to be addressed. Although existing algorithms may demonstrate excellent performance when dealing with single or specific types of interference, their efficacy often significantly degrades in practical applications characterized by the superposition of multiple interferences and dynamic environmental changes, thereby failing to meet practical application demands.

D. Scope of this Investigation

Addressing the aforementioned challenges, this study aims to enhance the robustness of continuous heartbeat detection for a specific individual using FMCW radar in typical interference environments. This investigation presents a phase error correction and heartbeat event probability prediction enhanced FMCW radar vital signs monitoring technique. Firstly, a radar echo signals reinforcement and high-SNR extraction framework is proposed to obtain high quality phase signal of vital signs. Then, an adaptive dual-sliding window phase error correction method is proposed to handle human body movements and environmental interference. And finally, a sequence-to-sequence DNN is developed to process the input weak phase signal and output the corresponding heartbeat event probability sequence for heart rate detection, which enhances the algorithm's tolerance to noise and adaptability to complex conditions.

III. Proposed Solution

To accurately extract the weak vital sign signals from radar data and achieve high-accuracy vital signs estimation, this section presents the proposed FMCW radar vital signs monitoring technique enhanced by phase error correction and neural network heartbeat event probability prediction.

A. A Multi-Stage Framework for Signal Processing

The proposed solution is a multi-stage algorithmic framework, as shown in Figure 1, primarily comprising three stages: radar data pre-processing, adaptive vital signs signal decomposition, and neural network heartbeat event probability prediction. The specific workflow includes:

1) Target radar data pre-processing: This stage is dedicated to processing raw radar data and isolating the phase signal reflected from a specific human target. Initially, after the radar's radio frequency (RF) operation and processing stages, an Intermediate Frequency (IF) signal is obtained, and the range-angle spectrum is computed based on Multiple-Input Multiple-Output (MIMO) data to determine the target's range bin and angle bin. The Minimum Variance Distortionless Response (MVDR) beamforming, based on MIMO antenna arrays, is employed to spatially filter out interference and focus on the desired individual in multi-target environments or cluttered scenarios. Subsequently, the phase signal at the target's location is extracted. An adaptive dual-sliding window phase error correction method is applied to identify and correct pulse spikes and segmental disturbances, thereby generating a clean and stable phase signal corresponding to chest displacement.

2) Adaptive vital sign decomposition: The enhanced chest wall undulation phase signal obtained from the previous stage is utilized and decomposed into respiratory and heartbeat components. An adaptive VMD method is employed, optimized by analyzing the decomposition residual energy and

maximizing the energy significance of the heartbeat mode, to determine the number of modes and the penalty factor. The respiration mode is used to directly calculate the respiration rate, while the heartbeat mode serves as the input for the subsequent neural network-enhanced heartbeat prediction.

3) Neural network heartbeat event probability prediction: A DNN with a hybrid architecture, based on a CNN encoder-decoder, a Transformer module, and a Long Short-Term Memory (LSTM) network, is used for heartbeat event probability prediction. This model does not directly perform the heartbeat event classification task but instead predicts a sequence of heartbeat event probabilities from longer segments of the heartbeat signal. The key advantage of this probability-based prediction method is its ability to leverage richer contextual information to identify complex interference patterns and flexibly handle signal noise and uncertainty through non-binary probabilistic outputs, thereby avoiding the rigid misclassifications common in traditional classification tasks when dealing with ambiguous signals. The CNN encoder extracts local spatial-temporal features, the Transformer captures temporal dependencies in the vital signs, and the Long Short-Term Memory (LSTM) models the temporal dynamics of each detected event and shapes its probability waveform. This architecture leverages the Transformer's strength in modeling global, long-range dependencies via self-attention, while utilizing the LSTM's recurrent nature to precisely model the local, step-by-step evolution of an event. The output probability sequence then undergoes regularized post-processing to yield final high-precision heart rate data.

The proposed multi-stage signal processing method systematically addresses challenges at various levels, from raw data acquisition to complex signal identification, aiming to provide a robust and accurate non-contact vital signs monitoring solution. The subsequent sub-sections elaborate on the principles and implementation methods of each stage within this framework.

B. Principle of FMCW Radar Vital Signs Detection

FMCW radar transmits periodic frequency-modulated signals, namely chirps, and receives echoes reflected from a target. Within the period of one chirp, the instantaneous frequency of the transmitted signal is expressed as:

$$f_T(t) = f_c + Kt \tag{1}$$

where f_c is the chirp starting frequency, and K is the frequency modulation slope, determined by the ratio of the total bandwidth to the chirp duration. The phase of the transmitted signal is then the integral of the frequency over the chirp duration:

$$\phi_T(t) = 2\pi\int_0^t (f_c + K\xi)d\xi = 2\pi f_c t + \pi K t^2 + \phi_0 \tag{2}$$

where ϕ_0 is the initial phase of the transmitted signal. For simplification, it is assumed to be $\phi_0 = 0$ henceforth. Thus, the transmitted signal is given by:

$$S_T(t) = A_T\cos[\phi_T(t)] = A_T\cos(2\pi f_c t + \pi K t^2) \tag{3}$$

where A_T is the amplitude of the transmitted signal. The transmitted signal is reflected by the target surface, and the received signal is an attenuated and delayed version of the transmitted signal. The time-of-flight delay produced by the i-th target in space is expressed as:

$$\tau_i = \frac{2R_i}{c} \tag{3}$$

where R_i is the distance between the radar and the target, and c is the speed of light. The received signal generated by reflection from the i-th target is then expressed as:

$$S_{R,i}(t) = \cos[\phi_{R,i}(t)] = A_{R,i}\cos[2\pi f_c(t-\tau_i) + \pi K(t-\tau_i)^2] \tag{4}$$

where $A_{R,i}$ is the amplitude of the received signal. The transmitted signal and the received signal are mixed, and then an output signal is generated, which is given by:

$$\begin{aligned} S_{out,}(t) &= S_T(t)S_{R,i}(t) \\ &= A_T A_{R,i}\cos(\phi_T(t))\cos(\phi_{R,i}(t)) \\ &= \frac{A_T A_{R,i}}{2}[\cos(\phi_T(t)-\phi_{R,i}(t)) + \cos(\phi_T(t)+\phi_{R,i}(t))] \end{aligned} \tag{5}$$

where,

$$\phi_T(t) = 2\pi f_c t + \pi K t^2 \tag{6}$$

$$\phi_{R,i}(t) = 2\pi f_c(t-\tau_i) + \pi K(t-\tau_i)^2 \tag{7}$$

Subsequently, low-pass filtering is applied to remove the high-frequency terms, retaining the difference frequency term, yielding the IF signal produced by the i-th target, expressed as:

$$\begin{aligned} S_{IF,i}(t) &= A_{IF,i}\cos(\phi_T(t) - \phi_{R,i}(t)) \\ &= A_{IF,i}\cos(2\pi K\tau_i t + 2\pi f_c\tau_i - \pi K\tau_i^2) \end{aligned} \tag{8}$$

where, under ideal conditions, $A_{IF,i}=A_T A_{R,i}/2$. The frequency of this IF signal is proportional to the target distance. By performing the FFT on the IF signal, the spectrum of the IF signal can be obtained. The spectral peak corresponds to the signal frequency term, $f_{IF,i}$, from which the distance R_i of target i can be calculated, thus determining the target's range bin.

The phase term $\varphi_{IF,i}$ of the IF signal can be used to detect subtle displacements of the target, expressed as:

$$\begin{aligned} \varphi_{IF,i} &= 2\pi f_c\tau_i - \pi K\tau_i^2 \\ &= \frac{4\pi f_c R_i}{c} - \frac{4\pi K R_i^2}{c^2} \\ &= \frac{4\pi R_i}{\lambda_c} - \frac{4\pi K R_i^2}{c^2} \end{aligned} \tag{9}$$

where λ_c is the wavelength of the electromagnetic wave corresponding to the center frequency f_c. The impact of subtle displacements caused by the target's vital signs on the distance is expressed as:

$$R_i = R_{0,i} + \Delta R_i(t) \tag{10}$$

where $R_{0,i}$ represents the fixed position of the i-th target relative to the radar, and $\Delta R_i(t)$ represents the subtle chest wall displacements caused by vital signs. In $\varphi_{IF,i}$, the quadratic term with respect to R_i has a minimal effect on phase changes, so it can be approximated that the phase primarily related to displacement is:

$$\varphi_{IF,i} = \frac{4\pi R_i}{\lambda_c} \tag{11}$$

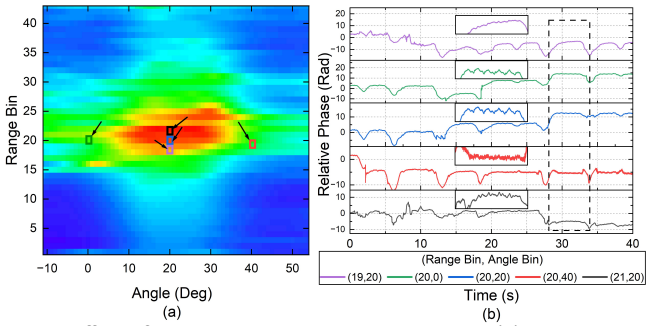

Fig. 2. Effect of target localization on signal quality: (a) Range-angle heatmap of the target region; (b) Raw phase signal sequences extracted from different range-angle combination positions.

The periodic components within this phase signal constitute the target's vital sign signals. In practical applications, IQ quadrature demodulation is typically employed during the mixing stage to avoid issues such as phase ambiguity and mirror image interference during the demodulation process.

C. Beamforming Spatial Filtering & Object Determination

To acquire vital signs information of a specific individual in space, beamforming techniques are required to suppress interference from other angular directions. This investigation employs an MVDR beamformer for spatial filtering. The MVDR beamformer is an adaptive beamforming algorithm, in principle, to maintain distortionless reception of the signal from the desired direction while minimizing the total output power of interference and noise from other directions. For signal $x(t)$ received by N antennas at the target's range bin, the output of the beamformer is $y(t)=w^H x(t)$. The optimal weight vector w is expressed as:

$$w = \frac{R_{xx}^{-1} a(\theta_0)}{a^H(\theta_0) R_{xx}^{-1} a(\theta_0)} \tag{12}$$

where $R_{xx}=E[x(t)x^H(t)]$ is the covariance matrix of the signal $x(t)$, assuming the DC component has been removed. $E[\bullet]$ denotes the expectation operation, $a(\theta_0)$ is the steering vector corresponding to the angle θ_0 derived from the antenna array parameters, and $(\bullet)^H$ denotes the conjugate transpose. Applying the obtained weight vector w to the signals received by the antenna array from the designated target's range bin can enhance the target signal and suppress sidelobe interference.

Several target candidate positions exist in the range-angle spectrum, and the selection of different range and angle bins significantly affects the signal quality. As shown in Figure 2, the optimal signal position for this measurement is located at range bin 20. The waveform from this bin exhibits a respiratory signal with a relatively large amplitude and regular periodicity, overlaid with a heartbeat signal of smaller amplitude and higher frequency. Regarding the selection of the range bin, bins closer than the optimum risk superficial sampling may fail to adequately capture weak surface vibrations like heartbeat. Further bins, however, suffer from interference due to deep-tissue reflections and significant attenuation of the heartbeat signal through tissue penetration. For the angle bin, if the radar beam's pointing angle deviates from the cardiac region, the strength of the heartbeat signal is attenuated. To effectively extract phase changes induced by the target's chest displacement, this method positions the signal analysis point near the center of the target region in the range-angle heatmap, and finely adjusts towards the surface of the target's chest closer to the radar. This approach prioritizes the capture of radar echoes generated by the chest wall surface, thereby minimizing signal interference from factors such as reflections from deep torso tissues and yielding a more direct and cleaner representation of the subtle chest wall movements.

D. Adaptive Dual Sliding Window Phase error correction

Through the processes described above, the algorithm obtains the radar phase information corresponding to the vital signs of the designated individual. However, due to the inherent high sensitivity of millimeter-wave radar signals to subtle disturbances during phase extraction, they are highly susceptible to various influencing factors, including interference from moving objects in the environment, body micro-motions, and external electromagnetic interference. These interferences primarily manifest in two key forms: firstly, as isolated, instantaneous impulsive spikes with amplitudes significantly exceeding the normal physiological signal range; and secondly, as episodic or segmental disturbances of relatively longer duration. The latter form of interference is persistent. It typically begins with a significant, large amplitude jump in its initial phase, which is then followed by a series of continuous fluctuations. Although these fluctuations may have a smaller amplitude, they are still strong enough to corrupt the true physiological information. Such distortions are randomly superimposed onto signal segments, impairing the identification of periodic components. This severely degrades the phase signal quality, presenting a formidable challenge for the subsequent accurate acquisition of vital signs and the effective analysis of physiological states. Isolated spikes and persistent disturbances usually coexist. Due to its suboptimal performance, the single-threshold method often either misses subtle interferences or generates false alarms in clean signal segments, which may corrupt the useful signal. To effectively mitigate the detrimental impact of the aforementioned interferences on phase signal integrity, an adaptive dual sliding window phase error correction method is proposed. This method is designed to dynamically identify and process segments affected by interference.

1) Interference segment identification and initiation of phase error correction: The algorithm monitors the phase increment across a sliding interference identification window in real-time. This increment, $\Delta\varphi_i=|\varphi_i-\varphi_{i\text{-}Nenter}|$, is calculated as the absolute difference between the current phase sample φ_i and the phase sample $\varphi_{i\text{-}Nenter}$ from the previous N_{enter} samples. When $\Delta\varphi_i$ exceeds a pre-defined entry threshold T_{enter}, the segment is identified as a potentially interfered one, and phase error correction is initiated.

2) Interference segment phase error correction and adaptive window expansion: Once an interference segment is entered, the algorithm initiates an interference processing window of dynamic length, which expands adaptively when new samples are incorporated. Within this window, the system applies more stringent checks and corrections for phase jumps. If the instantaneous phase change, $\Delta\varphi_j=|\varphi_j-\varphi_{j\text{-}1}|$, at any sample point j exceeds an intra-interference processing threshold T_{Process}, that sample is considered to be disturbed. The algorithm then corrects the phase by subtracting this increment $\Delta\varphi_j$ from sample point j and all subsequent samples in the current

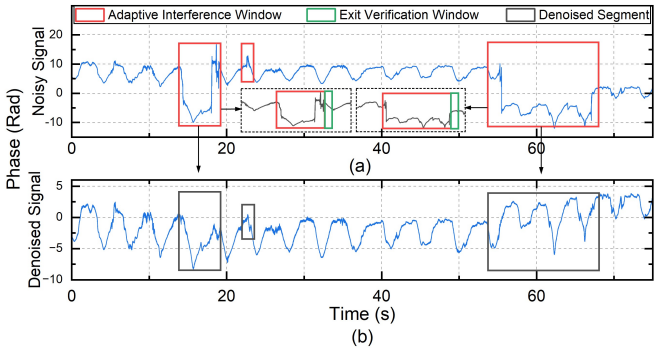

Fig. 3. Adaptive dual sliding window phase error correction method: (a) Interference patterns in the original phase signal and the dual sliding window processing mechanism; (b) Phase signal after processing with the adaptive dual sliding window phase error correction.

processing segment to smooth the offset caused by the disturbance.

3) Determination of interference segment end and exit from phase error correction: To ensure accurate identification of the interference segment and timely exit from the processing mode which could prevent over-correction of normal signal portions, an exit detection sliding window of fixed length N_{Exit} is employed. This exit detection window continuously assesses whether any instantaneous phase change $\Delta\varphi_k=|\varphi_k-\varphi_{k-1}|$ within it exceeds an exit threshold T_{Exit}. If $\Delta\varphi_k<T_{\text{Exit}}$ consistently holds for all sample points k within a complete N_{Exit} window, the interference segment is recognized to be completed, and the signal is considered stable. The algorithm then exits the interference processing mode and returns to the standard data processing pipeline.

Through this adaptive dual sliding window collaborative mechanism, the logical transitions of the interference processing are implemented by the joint control of T_{Enter}, T_{Process}, and T_{Exit}. For isolated phase spikes with very short duration, the algorithm applies the correction and then promptly exits the interference processing mode, resulting in a localized and transient impact. For longer-lasting, segmental interferences, the dynamically expanding processing window and the more stringent intra-segment processing threshold ensure that the interference is more comprehensively suppressed. Compared to methods employing a single global threshold, this approach provides more refined processing and causes less influence on unaffected signal portions. The parameters mentioned above are generally determined based on the measurement environment and the sampling rate. In complex environments, it is common to use a lower T_{Enter} to catch more potential disturbances and a lower T_{Exit} to be more confident that the disturbance has passed. Conversely, in ideal conditions without strong interference, a higher T_{Enter} and T_{Exit} are often employed. The guideline of T_{Process} selection is to make sure there is no missing interference within a disturbed segment.

Figure 3 illustrates typical phase disturbance patterns and the operational principle of the proposed algorithm. The red window denotes an interference segment, which includes both impulsive and segmental disturbances, and adaptively expands to incorporate all the detected disturbances. The green window represents the exit detection window, where the interference processing mode is terminated if no interference is detected for N_{Exit} consecutive samples within this window. The black window shows the outcome of the disturbance correction, validating the algorithm's effectiveness in handling both isolated impulsive and segmental disturbances.

E. Adaptive Mode Decomposition of Vital Sign Signals

When the stable and accurate chest surface displacement signal denoted by $x(t)$ is obtained in the pre-processing stage, the subsequent task is the reconstruction of respiration and heartbeat signals.

Chest wall displacements resulting from respiration and heartbeat modulate the radar's electromagnetic wave signal, which are ultimately regarded as specific modulated components within the phase signal. To efficiently extract and reconstruct high-quality respiration and heartbeat signals from the chest displacement signal, a crucial aspect is to ensure the effective separation and capture of these physiological signal components. This section employs an adaptive processing algorithm for vital signs signal decomposition utilizing VMD. In this approach, the number of modes K and the bandwidth characteristics of each mode are optimized via an adaptive strategy, and the relevant vital sign frequency bands are automatically selected.

The method firstly decomposes $x(t)$ using VMD into K IMFs, denoted as $u_k(t)$, each possessing a specific center frequency ω_k. The VMD decomposition is accomplished by formulating an optimization model that concurrently minimizes the spectral bandwidth of these modes while ensuring their sum reconstructs the original signal. This is achieved by solving the following constrained variational problem:

$$\min_{\{u_k\},\{\omega_k\}}\left\{\sum_{i=1}^{K}\left\|\partial_t\left[\left(\delta(t)+\frac{j}{\pi t}\right)*u_k(t)\right]e^{-j\omega_k t}\right\|_2^2\right\} \quad \text{s.t.}\sum_{i=1}^{K}u_k(t)=x(t) \tag{13}$$

where $\delta(t)$ is the Dirac delta function, * denotes convolution. The overall objective is to minimize the sum of the bandwidths of each IMF, subject to the constraint that the sum of the modes reconstructs the original signal $x(t)$. To solve this variational problem, VMD introduces an Augmented Lagrangian. In this Augmented Lagrangian, α acts as the weighting factor for the quadratic penalty term, ensuring the fidelity of the original signal's reconstruction from the sum of the decomposed modes, while also influencing the bandwidth of each mode.

To ensure that VMD captures sufficient total signal energy, while also considering the prominence of spectral peaks within different modes, is a prerequisite for the accurate subsequent extraction of vital sign signals. To optimize this decomposition process, K and α are adaptively adjusted according to the signal characteristics. The normalized residual energy $E_{\text{res}}(K, \alpha)$ is employed to assess whether the decomposition has captured the principal energy of the signal, which is given by:

$$E_{res}(K,\alpha)=\frac{\left\|x(t)-\sum_{i=1}^{K}u_i(t;\alpha)\right\|_2^2}{\|x(t)\|_2^2} \tag{14}$$

where $u_i(t; \alpha)$ represents the IMF obtained with parameter α.

The algorithmic procedure is divided into three steps:

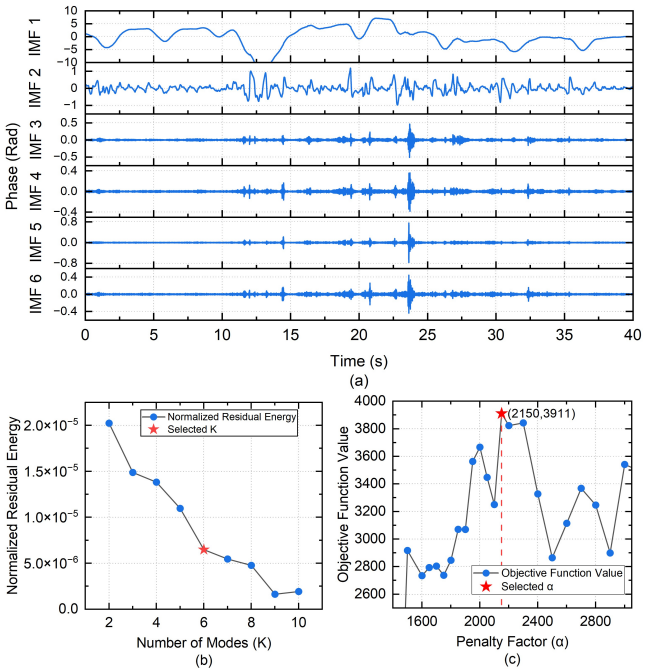

Fig. 4. Results of adaptive vital signs decomposition: (a) Time-domain signal of the 6 IMFs obtained through adaptive decomposition; (b) Curve of normalized residual energy versus the preset number of decomposition modes K, with α=1800; (c) Curve of the objective function J versus the penalty factor α.

1) Determination of mode number and initial decomposition: VMD is initially performed using an empirical value α_{init}. A candidate optimal number of modes K_{opt} is determined by identifying the elbow point of the curve plotting $R_{\text{res}}(K, \alpha_{\text{init}})$ against K, where K is less than the preset upper limit $K_{\max}$. This elbow point signifies that further increments in K provide diminishing marginal contributions to the reduction of residual energy. The default value for α_{init} is typically set to 1800 to accommodate most scenarios, though adjustments based on specific signal characteristics may be necessary in practical applications.

2) Candidate vital signs mode identification: For the K_{opt} IMFs resulting from the decomposition, the center frequency ω_k of each IMF $u_k(t)$ is analyzed. IMFs with center frequencies in the range 0.1–0.5 Hz are identified as candidate respiratory modes. The heartbeat mode is selected in the subsequent steps.

3) Heartbeat mode selection and α adaptive optimization based on energy significance: Based on the initial decomposition, an adaptive optimization strategy rooted in energy significance is proposed. The core idea is to quantify the prominence of the heartbeat signal within the spectrum of each mode, thereby identifying an optimal parameter α_{opt} to better isolate the heartbeat mode and refine the overall decomposition. Firstly, the maximum power spectral component of $u_k(t)$ within the heartbeat frequency band is calculated by:

$$P_{heart}(\alpha) = \max_{f \in [f_{h1}, f_{h2}]} \left\| S_k(f;\alpha) \right\|_2^2 \tag{15}$$

where f_{h1} and f_{h2} define the lower and upper bounds of the heartbeat frequency band, respectively, and $S_k(f; \alpha)$ is the power spectrum of $u_k(t)$ obtained with parameter α. Then, the total power of $u_k(t)$ across its entire effective frequency range is computed by:

$$P_{total}(\alpha) = \sum_{f=0}^{f_s/2} \left\| S_k(f;\alpha) \right\|_2^2 \tag{16}$$

where f_s is the radar's slow-time sampling rate. Finally, the relative peak energy ratio $R_k(\alpha)$ which represents the peak power within the heartbeat band relative to the total power of the mode is calculated. The $R_k(\alpha)$ quantifies the significance of the heartbeat component within that mode:

$$R_k(\alpha) = \frac{P_{heart}(\alpha)}{P_{total}(\alpha)} \tag{17}$$

The algorithm defines a search range for α and a search step $\Delta\alpha$. It iterates through α values within this range for each $u_k(t)$, aiming to maximize the objective function $J(\alpha)$ given by:

$$J(\alpha) = \frac{R_k(\alpha)}{E_{res}(\alpha) + \varepsilon} \tag{18}$$

where ε is a very small positive constant to prevent division by zero. A more prominent heartbeat component results in a larger $R_k(\alpha)$, while a more thorough decomposition yields a smaller $E_{\text{res}}(\alpha)$. The optimal decomposition parameter for the current signal segment denoted by α_{opt} is the α value that maximizes $J(\alpha)$. The mode $u_k(t)$ that maximizes $J(\alpha)$ is then identified as the heartbeat mode.

Figure 4(a) shows typical time-domain waveforms of the modes obtained by applying the adaptive vital sign decomposition algorithm to the target's chest displacement signal. These modes incorporate signals from various frequency scales present in the original signal. Figure 4(b) illustrates the curve of normalized residual energy plotted against the number of decomposition modes K, used during the preliminary determination of K. As observed in the figure, the normalized residual energy progressively decreases with the increase of K. The elbow point of this curve serves as the candidate K_{opt}, representing a balance between the capture of principal signal energy and the prevention of over-decomposition. Figure 4(c) shows the objective function J plotted against different values of α. The optimal α for the current signal segment is identified by locating the peak of J in this graph.

Given that the respiratory signal typically has a significant contribution and is less susceptible to interference, it is processed using the FFT. The frequency corresponding to the spectral peak in the FFT result is then determined as the target's respiration rate. For the heartbeat signal, however, the adaptive VMD optimizes the parameters K and α to collaboratively enhance mode separability. This approach can effectively suppress the crosstalk of respiratory harmonics into the heartbeat mode, thereby mitigating harmonic interference prior to subsequent neural network processing to yield a more accurate input.

F. Enhancing HR Accuracy with Probability Prediction

To achieve stable heart rate estimation, a heartbeat event probability prediction method is developed based on a novel deep neural network architecture, termed RTL-Unet. This method employs a relatively long observation window to predict the temporal probability distribution of heartbeat events, rather than outputting binary labels or performing instantaneous HR regression. Consequently, this approach

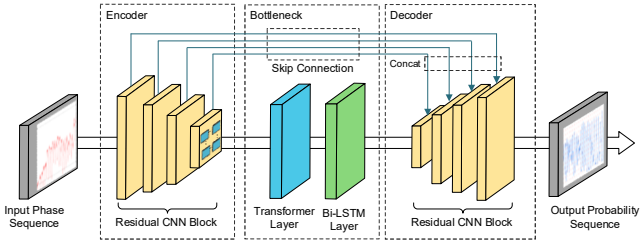

Fig. 5. Schematic diagram of the adopted neural network model.

enhances the tolerance of the network's output to noise and interference. For signal segments that are hard for the model to interpret due to superimposed interference, it could avoid binary classification errors by outputting a waveform of low confidence. Simultaneously, because longer windows offer richer contextual information, the model can analyze not only local signal morphology but also the overall trend of the time series. The incorporation of heartbeat periodicity and rhythmicity of the signals makes it appropriate for a more thorough analysis. The periodic trend of heartbeats is maintained within the long-window probability sequence, and random prediction fluctuations are suppressed, thereby allowing a more effective capture of the signal's dominant components.

The training data for this network comprises heartbeat mode phase sequences acquired using a 60GHz FMCW radar and processed with the algorithms described above. Synchronously collected ECG signals serve as the ground truth.

Data labels are generated from heartbeat events. Firstly, the discrete time points of ECG R-peaks are identified. Subsequently, Gaussian functions with a standard deviation of σ, centered at each R-peak time, are superimposed to create a smooth time series. This series represents the probability of a heartbeat event occurring at each sample point. The probability representation offers the network a smoother and more learnable reference, and it also facilitates the detection of subtle temporal shifts in heartbeat events.

The structure of the proposed RTL-Unet is illustrated in Figure 5. This hybrid network is designed to leverage the complementary strengths of several advanced deep learning components. Firstly, the input heartbeat sequence passes through an encoder based on a Convolutional Neural Network (CNN). This encoder is designed to learn local spatial-temporal features from the signal, extract effective representations, and progressively downsample the data. The encoder consists of four cascaded 1D convolutional residual modules. Subsequently, the feature sequence from the encoder is fed into a Transformer module, which leverages its self-attention mechanism to capture long-range vital signs dependencies and periodic patterns within the sequence. Its function is to identify and localize all potential heartbeat events within the input signal segment. The Transformer module, in particular, learns to differentiate the distinct temporal signatures of physiological heartbeats, such as rhythmic stability and morphological consistency, from respiratory harmonic artifacts, even when their frequencies overlap. Then, the feature sequence processed by the Transformer, which is now enriched with global information, is fed into an LSTM layer. LSTM is a type of Recurrent Neural Network (RNN) that has a key advantage of meticulously modeling the dynamic evolution and local dependencies of time series data. In this architecture, the LSTM layer is primarily responsible for delineating the precise shape of the probability distribution around each heartbeat instance. Finally, a decoder constructed with deconvolutional layers symmetrical to the encoder is employed at the network's output stage. In order to ensure the high-fidelity reconstruction of the probability sequence, the network adopts a U-Net-like structure, incorporating skip connections between the corresponding layers of the encoder and decoder. These connections allow low-abstraction-level, high-resolution features from the encoder to be directly fused into the decoder, which is critical for restoring precise temporal details. This decoder takes the feature sequence from the LSTM as well as the fused features from the skip connections, and then upsamples and maps it back to the temporal resolution of the original signal.This decoder takes the feature sequence from the LSTM, and then upsamples and maps it back to the temporal resolution of the original signal. This process ultimately yields the heartbeat event probability sequence, achieving a sequence-to-sequence mapping from the input radar phase sequence to the output heartbeat probabilities.

The objective of network training is to minimize the discrepancy between the predicted probability sequence $\hat{y}$ and the ground truth probability sequence y. This method utilizes a Weighted Mean Squared Error (WMSE) as the loss function. This loss function guides the model to prioritize the optimization of prediction accuracy in peak regions, which is achieved by assigning higher weights to sample points where the target probability values are greater. The loss function $\mathcal{L}_{\text{WMSE}}$ is defined as follows:

$$\mathcal{L}_{\text{WMSE}} = \frac{1}{N}\sum_{i=1}^{N}(1+\alpha y_i)(\hat{y}_i - y_i)^2 \tag{19}$$

where N is the number of signal points, y_i is the ground truth probability for the i-th point, $\hat{y}_i$ is the predicted probability for the i-th point, and α is a non-negative weighting factor. Model parameters are iteratively updated using the Adam optimizer, with appropriate configurations for learning rate, batch size, and training epochs for performance optimization.

To enhance the reliability of the output, post-processing is performed on the network's output. Firstly, a 50% threshold is applied to filter out low-probability peaks, thereby reducing the influence of potential noise. Secondly, to further eliminate predicted peak intervals inconsistent with physiological patterns, a time interval constraint reflecting valid physiological ranges is applied to the probability peaks. This step removes densely clustered probability peaks that do not align with physiological intervals. Finally, the frequency corresponding to the maximum spectral value in the probability sequence is determined using FFT, yielding the final heart rate estimation.

IV. Experimental Verification

To validate the feasibility, effectiveness, and ultimate vital signs monitoring performance of the proposed method, this section presents the experimental studies conducted.

A. Experimental Setup

Fig. 6. Experimental setup and the test scenario.

TABLE I
SPECIFICATION OF IWR6843ISK RADAR

Parameters	Value	Unit
Center frequency	60	GHz
Bandwidth	3.6	GHz
TX power	12	dBm
Antenna configuration	2Tx / 4Rx MIMO	
Chirp cycle duration	60	μs
Chirp repetition frequency	1000	Hz
ADC sampling rate	7.5	MSPS

The experimental setup, illustrated in Figure 6(a), was established with a millimeter-wave radar evaluation module IWR6843ISK (Texas Instruments, US) and a real-time data capture module DCA1000EVM (Texas Instruments, US). The IWR6843ISK is an integrated single-chip millimeter-wave sensor operating in the 60-64 GHz frequency band. In this investigation, the key parameters of the radar system are given in Table 1. After the radar echo signals undergo on-chip processing, the raw Analog-to-Digital Converter (ADC) sample data are acquired using the DCA1000EVM. The raw radar data are then transmitted to a host PC via the DCA1000EVM for subsequent processing.

The heartbeat response for reference was acquired using a single-lead ECG front-end module with an AD8232 (Analog Devices, US) and recorded in the host PC. The ground truth for respiration was controlled by instructing participants to breathe uniformly in accordance with a preset metronome.

The experiment was performed in a typical office environment, as shown in Figure 6(b), specifically a small-sized conference room of approximately 5 m × 10 m. This room was furnished with a conference table, chairs, and other standard office equipment. Participants were instructed to sit on a chair facing the radar. This environment was designed to embody clutters of stationary objects as well as multipath interference that is typically encountered in daily office scenarios. The space can accommodate movements of subjects. Attempts were made to assess the algorithm's robustness under real-world office conditions. 6 volunteers are recruited for the tests and informed consent were obtained.

This study was reviewed and approved by our institution and conducted in accordance with the principles of the Declaration of Helsinki. Prior to the experiment, all participants provided written informed consent after being fully briefed on the procedure's confirmed safety, which is ensured by the negligible RF exposure from a low transmission power of 12 dBm and an operating distance greater than 1.5 meters.

B. Verification of the Proposed Method

1) Respiration and Heartbeat Signal Extraction

To verify the effectiveness of the proposed method for target respiration and heartbeat signal extraction, as well as the adaptive dual sliding window phase error correction technique, the step-by-step results of the phase signal extraction process are presented in Figure 7.

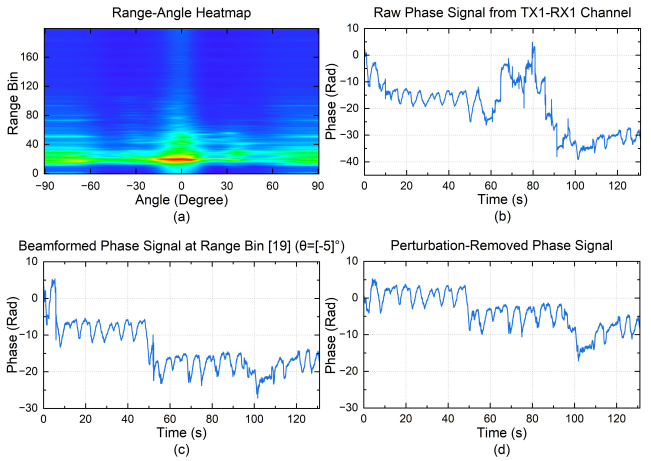

Fig. 7. Extraction of phase response: (a) Joint range-angle heatmap; (b) Phase response based on a Tx1-Rx1 single antenna pair; (c) Phase response from 2Tx-4Rx antenna array with beamforming; (d) Phase response of the 2Tx-4Rx antenna array after applying the adaptive dual sliding window for phase correction.

Figure 7(a) shows the joint range-angle heatmap, where the target's location is in high energy echo region. The target was identified at the range bin 19 with an angle of arrival of −5°. The differential phase shifts between a single pair of antennas (1 Tx and 1 Rx) , and the transmit array (2 Tx) and receive antenna array with beamforming (4 Rx) are depicted in Figures 7(b) and 7(c) respectively, the phase response over a time span of 130 s for the carrier frequency was monitored. Figure 7(d) illustrates the phase response after the correction processing is implemented on the beamformed signal. Compared to the signal obtained from a single antenna pair, the phase information as a result of the window processing on the received signal from the array after beamforming operation excluded anomalies caused by background noise and random disturbances, hence clearer periodic components can be observed, that are most likely attributable to respiration and heartbeat. These results validated the effectiveness of the proposed adaptive dual sliding window phase error correction method in suppressing phase signal noise and eliminating sharp jumps, demonstrating that this denoising approach can successfully improve the fidelity of phase responses.

2) Respiration and Heartbeat Signal Decomposition

Figure 8(a) and 8(c) present the time-domain sequence of the extracted respiratory mode and heartbeat mode obtained by adaptive vital signs signal decomposition, and Figure 8(b) and 8(d) show their corresponding spectrum. The spectral peak of respiration in Figure 8(b) agrees with the participant's instructed breathing rate of 9 Breaths Per Minute (BPM), set by a metronome. The results indicate that the frequency corresponding to the respiration mode that is obtained by adaptive vital signs signal decomposition provides an accurate respiratory rate estimation.

3) DNN Probability Prediction for Heart Rate Estimation

This subsection presents the prediction results on data collected from a single stationary subject. A segment of heartbeat-led responses in the time domain, namely phases are

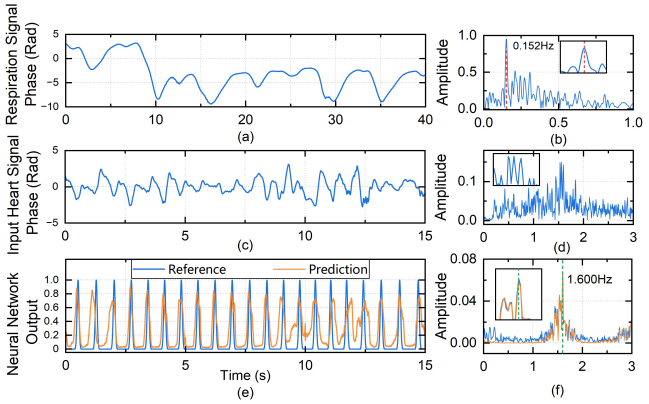

Fig. 8. Validation of DNN heartbeat event probability prediction: (a) Time-domain sequence of the respiratory signal mode; (b) Spectrum of the respiratory signal mode; (c) Time-domain sequence of the heartbeat signal mode; (d) Spectrum of the heartbeat signal mode; (e) Predicted heartbeat event probability sequence; (f) Spectrum of the predicted heartbeat event probability sequence.

illustrated in Figure 8(c), is fed into the neural network. Within the anticipated heartbeat frequency range of 0.8–2.5 Hz, the spectrum does not show a single and distinct peak. Instead, it reveals multiple interference peaks of similar amplitudes, making it a challenge for conventional peak-detection-based heart rate estimation algorithms to identify the dominant heartbeat frequency. After implementing the DNN model, Figure 8(e) presents the heartbeat event probability sequence predicted by the neural network, it largely overlapped with the reference probability sequence derived from the R-peak locations of the synchronously recorded ECG. The occurrence of peaks in the neural network outcome agrees fairly well with that in the reference. Based on this probability sequence, the heart rate was then determined by seeking the spectral peak. The resulting spectrum, shown in Figure 8(f), exhibits a good agreement with the ECG reference heart rate, thereby demonstrating the neural network model's effectiveness in accurately predicting heartbeat events and estimating the heart rate.

C. Vital Signs Detection Performance

To evaluate the adaptability of the proposed method to various complex scenarios encountered in practical applications, targeted experiments were conducted. These experiments investigated the impact of interference among different subjects, respiratory patterns and intensity changes, and physiological differences between individuals.

1) Evaluation of Specific Target Focusing Capability in Multi-Individual Scenarios

In practical monitoring environments, multiple individuals may present within the radar's field of view. The system is required to accurately extract the vital signs of a specific Target of Interest (ToI). The following multi-target scenarios were designed to evaluate the system's target identification and interference suppression capabilities in such situations:

- Scenario 1: The ToI was located in front of the radar with a distance and angle of 1.5m and 0°, with an interfering individual at 2.5 m and 15°.
- Scenario 2: The ToI was in the front with a distance and angle of 1.5m and -20°, with an interfering individual at the same distance but an angle of 20°.
- Scenario 3: The ToI was at 1.5m and 0°, with an interfering individual in very close proximity.

In each of the above scenarios, the system was configured to extract only the vital signs of the ToI. Figure 9 shows the system's monitoring results under these multi-target conditions. Specifically, Figures 9(a), 9(c), and 9(e) show the joint range-angle heatmaps for the three scenarios, respectively. Figures 9(b), 9(d), and 9(f) provide spectral comparisons between the predicted target heartbeat signals and the reference heartbeat signals for each scenario, annotated with absolute error and absolute percentage error. Figure 9(g) shows the statistical error across 30 measurements for each of these three conditions. Evidently, the proposed method can effectively identify the ToI and achieve high-accuracy heart rate estimations in the common multi-individual interference scenarios, thus validating its effectiveness. Since the echo signal incorporates the vital sign signals of all the individuals in the radar's coverage, any individual can be identified as the ToI by selecting the proper range and angle bin, which could finally achieve the simultaneous monitoring of multiple targets.

2) System Stability Assessment under Varying Respiratory Patterns and Micro-motion Interference

Dynamic changes in human respiratory patterns such as deep breathing, shallow breathing, and breath-holding along with body micro-motions like slight postural adjustments or coughing, are common interference sources that can significantly degrade the quality of extracted heartbeat signals.

The experiment was designed with a single participant positioned 1.5 meters from the radar at 0° direction, performing the following four typical respiratory patterns in sequence:

- Short breath-hold and cough: The participants held their breath for 15 seconds, then resumed normal uniform breathing, with coughing during the recovery.
- Rapid shallow breathing: High respiratory frequency with small chest displacement amplitude.
- Normal breathing: Calm and uniform breathing under normal physiological conditions.
- Slow deep breathing: Low respiratory frequency with significant chest displacement amplitude.

The results of the proposed method under these test conditions are shown in Figure 10. Figure 10(a) presents the time-domain sequences of the pre-processed chest displacement signals obtained under the four specified respiratory patterns and micro-motion interferences. Figure 10(b) shows the scatter plots, derived from 40 repeated measurements for each condition, comparing the agreement between heart rates estimated under these varying respiratory patterns and the synchronously recorded reference values. The results demonstrate that the outcomes of multiple measurements closely approximate the $Y=X$ line across various heart rates and respiratory patterns, indicating that the proposed method exhibits robust estimation accuracy and stability under the influence of diverse respiratory modes.

3) Impact of Inter-Individual Physiological Differences on System Performance

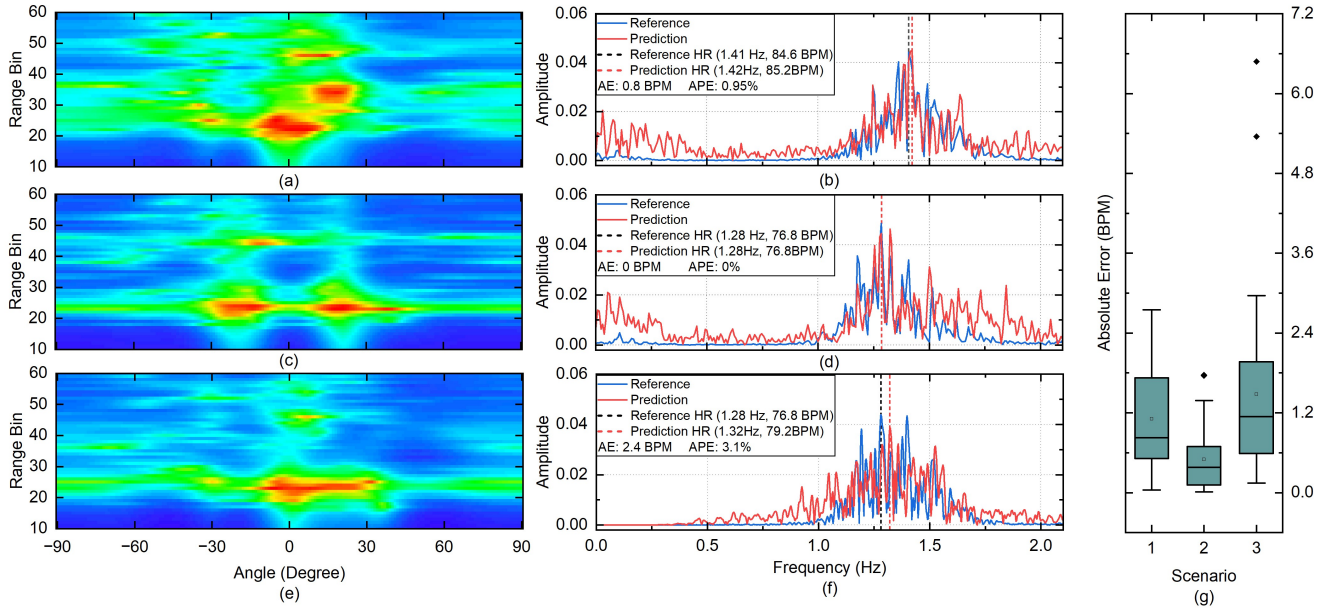

Fig. 9. Evaluation results of specific target focus capability in multi-individual scenarios: (a) Scenario 1 joint range-angle heatmap; (b) Scenario 1: predicted target heartbeat spectrum and reference signal spectrum; (c) Scenario 2 joint range-angle heatmap; (d) Scenario 2: predicted target heartbeat spectrum and reference signal spectrum; (e) Scenario 3 joint range-angle heatmap; (f) Scenario 3: predicted target heartbeat spectrum and reference signal spectrum; (g) Error distribution of 30 measurements.

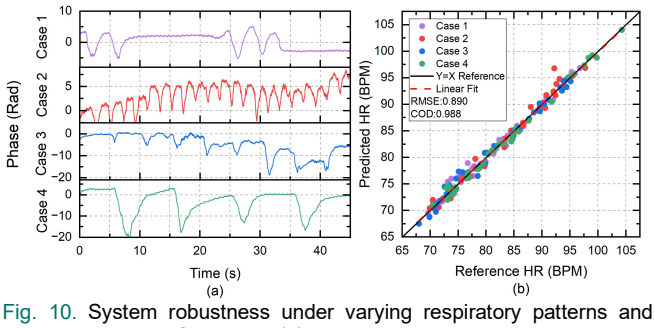

Fig. 10. System robustness under varying respiratory patterns and micro-motion interferences: (a) Target chest displacement phase sequences under different respiratory patterns; (b) Distribution of predicted results versus reference results from 40 measurements under different respiratory patterns.

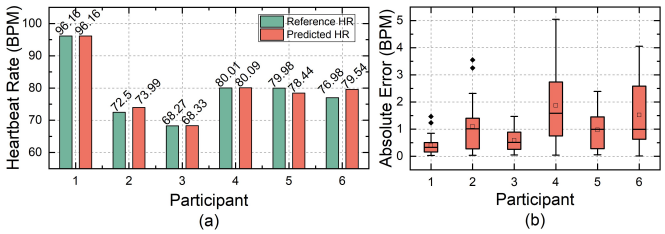

Fig. 11. Assessment of the impact of inter-individual physiological differences on system performance: (a) Comparison of predicted heart rate with reference heart rate during long-term single continuous monitoring; (b) Absolute heart rate errors distribution of 30 times short-term repeated monitoring sessions.

Variations in physiological structure, body type, and breathing habits among individuals can lead to different characteristics in their vital sign signals. These differences can, in turn, impact the generalizability of methods for extracting vital sign parameters. To evaluate the system's adaptability and measurement consistency across different subjects, two sets of experiments were performed with 6 participants: Firstly, a single 3-minute continuous vital signs monitoring session; and secondly, 30 times 30-second vital signs monitoring sessions. During the experiments, participants were positioned 1.5 meters from the radar at a 0° direction.

Figure 11(a) presents the absolute heart rate errors for the 6 different participants during the single long-term continuous monitoring session, which aimed at evaluating the system's stability over extended periods for different individuals. Figure 11(b) illustrates the distribution of absolute heart rate errors for each participant across 10 repeated short-term monitoring tasks. The measurement results indicate that the system exhibits good stability across different individuals and various measurement instances, and the proposed algorithm demonstrates strong adaptability to inter-individual physiological differences.

D. Discussion

In summary, the proposed method consistently achieved a Mean Absolute Error (MAE) in the range of 0.3-1.9 Beats Per Minute (BPM) with a median absolute error in 0.4-1.6 BPM, and an Absolute Percentage Error (APE) in the range of approximately 0.5%-2.9% across the various experimental scenarios. For a comparative performance evaluation, the proposed algorithm was benchmarked against existing algorithms, such as CWT, FFT, EWT, and VMD, using the same dataset. The results depicted in Figure 12 demonstrate that the proposed method achieves lower absolute errors and a more concentrated error distribution for heart rate estimation. Furthermore, it exhibits superior stability across multiple measurements and greater consistency. These findings indicate that, compared to the existing radar-based vital signs monitoring signal processing techniques, the proposed method demonstrates competitive performance.

Regarding algorithmic efficiency, our proposed method is sufficiently fast for real-time implementation. Its main components consist of MVDR beamforming, phase error correction, adaptive VMD, and neural network inference. The phase error correction step is a linear process with a time complexity directly proportional to the signal length, resulting

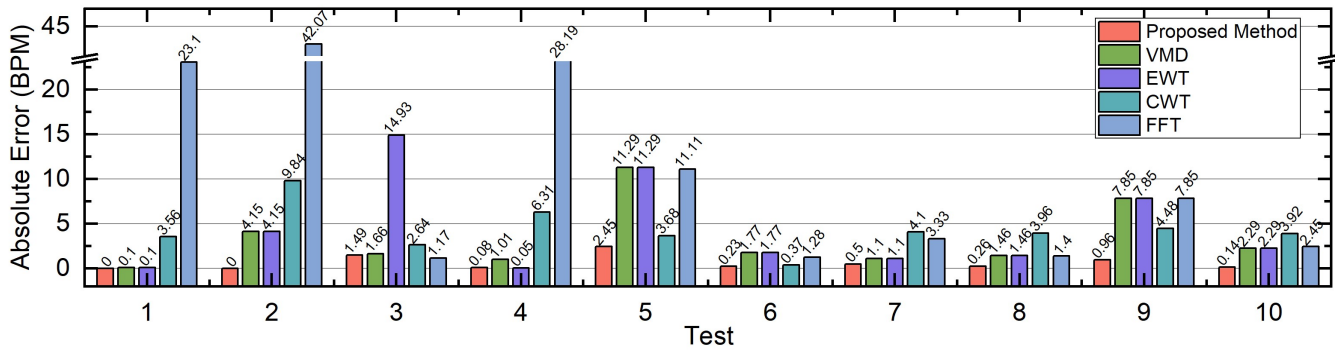

Fig. 12. Comparison of heart rate extraction performance with existing methods.

in negligible processing cost. The other key components including beamforming, adaptive VMD, and neural network inference rely on matrix multiplication, FFT, and bounded-region searches, and their performance is significantly accelerated through parallel processing. Our experiments have verified that the algorithm runs in real-time on both PCs and edge devices, confirming its applicability in practice.

In the current body of research in this domain, recently published studies typically report heart rate MAE in the range of 0.5–3 BPM. Under more challenging conditions, this error can increase to 5–6 BPM [33,41], or a Mean APE (MAPE) in 0.6%–4% [22,39]. The method proposed in this study, leveraging target phase error correction, adaptive vital sign signals decomposition, and deep learning-based heartbeat event probability prediction, enhances the vital signs detection performance against complex environmental interferences. Even when facing challenging scenarios such as multi-individual aliasing from proximate individuals, strong multipath interference, and phase distortions due to human micro-motions, it can consistently maintain comparable or superior measurement accuracy and demonstrates stable performance across diverse settings.

V. Conclusions and Future Work

This study addresses the entanglement between different vital signs, and interference among several targets that FMCW radar encounters in vital signs monitoring, particularly in heartbeat detrmination, factors including human micro-motions, high-order respiratory harmonics overlapping, environmental clutter, and the inherent sensitivity of phase responses are imposing serious challenges. A multi-stage data processing framework with phase error correction and heartbeat event probability prediction for FMCW radar vital signs monitoring is developed with experimental verification. The experimental results have demonstrated its capability to maintain high measurement accuracy and stability even when facing complex scenarios involving multi-individual signal overlapping, strong multipath propagation, and interference from human micro-motions. Comparative results against existing benchmark algorithms have demonstrated its superiority regarding absolute error and the concentration of error distribution in heart rate estimation of the proposed solution.

Despite the positive progress achieved in this investigation, some limitations persist, which have also raised directions for future investigation. Firstly, when the human body performs significant motions, the current method struggles to extract adequate information to serve as input for the neural network and consequently fails to produce meaningful output. This limitation remains a key challenge for future research. Secondly, the performance of the DNN models is dependent on the quantity and diversity of training data. Although the effectiveness of the model has been experimentally validated in this study, future efforts should be devoted to data collection and testing across populations with broader variations in age, body types, and health conditions under a wider range of environmental settings. Such endeavors are crucial for improving the model's generalization capabilities and its practical use in different applications.

References

[1] B. J. Drew et al., "Practice standards for electrocardiographic monitoring in hospital settings," *Circulation*, vol. 110, no. 17, pp. 2721-2746, 2004.

[2] T. Desquins, F. Bousefsaf, A. Pruski, and C. Maaoui, "A survey of photoplethysmography and imaging photoplethysmography quality assessment methods," *Appl. Sci.*, vol. 12, Art. no. 9582, 2022.

[3] L. Scalise and U. Morbiducci, "Non-contact cardiac monitoring from carotid artery using optical vibrocardiography," *Med. Eng. Phys.*, vol. 30, no. 4, pp. 490-497, 2008.

[4] S. Ahmed, K. D. Kallu, S. Ahmed, and S. H. Cho, "Hand gestures recognition using radar sensors for human-computer-interaction: A review," *Remote Sens.*, vol. 13, no. 3, Art. no. 527, 2021.

[5] C. Huan, P. Kontou, S. Ben Smida and D. E. Anagnostou, "Dual-band CW radar system for vital signs detection with interference cancellation method," *IEEE Trans. Microw. Theory Techn.*, vol. 73, no. 6, pp. 3581-3596, Jun. 2025.

[6] X. Ma, "Design of a 100-GHz double-sideband low-IF CW Doppler radar transceiver for micrometer mechanical vibration and vital sign detection," *IEEE Trans. Microw. Theory Techn.*, vol. 68, no. 7, pp. 2876–2890, Jul. 2020.

[7] S. Yao, J. Cong, D. Li and Z. Deng, "Noncontact vital sign monitoring with FMCW radar via maximum likelihood estimation," *IEEE Internet Things J.*, vol. 11, no. 23, pp. 38686-38703, Dec. 2024.

[8] Y. Wang, W. Wang, M. Zhou, A. Ren, and Z. Tian, "Remote monitoring of human vital signs based on 77-GHz mm-wave FMCW radar," *Sensors*, vol. 20, no. 10, Art. no. 2999, May 2020.

[9] G. Sacco, E. Piuzzi, E. Pittella, and S. Pisa, "An FMCW radar for localization and vital signs measurement for different chest orientations," *Sensors*, vol. 20, no. 12, Art. no. 3489, Jun. 2020.

[10] J. Jung, S. Lim, J. Kim and S. -C. Kim, "Non-line-of-sight vital sign detection using multipath propagation of UWB radar," *IEEE Antennas Wireless Propag. Lett.*, vol. 23, no. 7, pp. 2219-2223, Jul. 2024.

[11] D. Yang, Z. Zhu, J. Zhang, and B. Liang, "The overview of human localization and vital sign signal measurement using handheld IR-UWB through-wall radar," *Sensors*, vol. 21, no. 2, Art. no. 402, Jan. 2021.

[12] L. Qiao et al., "Learning-refined integral null space pursuit algorithm for noncontact multisubjects vital signs measurements using SFCW-UWB

and IR-UWB radar," *IEEE Trans. Instrum. Meas.*, vol. 71, pp. 1-13, Oct. 2022.
[13] C. A. Schroth et al., "Emergency response person localization and vital sign estimation using a semi-autonomous robot mounted SFCW radar," *IEEE Trans. Biomed. Eng.,* vol. 71, no. 6, pp. 1756-1769, Jun. 2024.
[14] J. Liu, F. Tong and C. Gu, "Non-contact vital sign detection with high noise and clutter immunity based on coherent low-IF CW radar," *IEEE J. Electromagn., RF, Microw. Med. Biol.*, vol. 9, no. 1, pp. 90-100, Mar. 2025.
[15] M. Farooq et al., "Contactless heart sound detection using advanced signal processing exploiting radar signals," *IEEE J. Biomed. Health Informat.*, vol. 29, no. 2, pp. 1009-1020, Feb. 2025.
[16] Y.-H. Lin, J.-H. Cheng, L.-C. Chang, W.-J. Lin, J.-H. Tsai, and T.-W. Huang, "A broadband MFCW agile radar concept for vital-sign detection under various thoracic movements," *IEEE Trans. Microw. Theory Techn.*, vol. 70, no. 8, pp. 4056–4070, Aug. 2022.
[17] W. Xue, R. Wang, L. Liu, and D. Wu, "Accurate multi-target vital signs detection method for FMCW radar," *Measurement*, vol. 223, Art. no. 113715, Dec. 2023.
[18] E. Antolinos and J. Grajal, "Comprehensive comparison of continuous-wave and linear-frequency-modulated continuous-wave radars for short-range vital sign monitoring," *IEEE Trans. Biomed. Circuits Syst.*, vol. 17, no. 2, pp. 229–245, Apr. 2023.
[19] L. Kouhalvandi and S. Karamzadeh, "Advances in non-contact human vital sign detection: A detailed survey of radar and wireless solutions," *IEEE Access*, vol. 13, pp. 27833–27851, 2025.
[20] S. Dong et al., "A review on recent advancements of biomedical radar for clinical applications," *IEEE Open J. Eng. Med. Biol.*, vol. 5, pp. 707-724, 2024.
[21] Q. Zhai, X. Han, Y. Han, J. Yi, S. Wang and T. Liu, "A contactless on-bed radar system for human respiration monitoring," *IEEE Trans. Instrum. Meas.*, vol. 71, pp. 1-10, 2022.
[22] Z. Wang, C. Li, S. Tu, and Z. Liu, "A novel rotary FMCW radar for omnidirectional multiperson localization and vital signs detection," *IEEE Trans. Microw. Theory Techn.*, vol. 72, no. 3, pp. 1886–1899, Mar. 2024.
[23] Z. Xu, T. Ye, L. Chen, Y. Gao, and Z. Chen, "Health-radar: Noncontact multitarget heart rate variability detection using FMCW radar," *IEEE Sens. J.*, vol. 25, no. 1, pp. 405–418, Jan. 2025.
[24] D. Uzunidis, S. A. Mitilineos, C. Ponti, G. Schettini and C. Z. Patrikakis, "Detection of trapped victims behind large obstacles using radar sensors: A review on available technologies and candidate solutions," in *Proc. IEEE Conf. Antenna Meas. Appl. (CAMA)*, Genoa, Italy, Nov. 2023, pp. 1025-1030.
[25] T. K. V. Dai, Y. Yu, P. Theilmann, A. E. Fathy and O. Kilic, "Remote vital sign monitoring with reduced random body swaying motion using heartbeat template and wavelet transform based on constellation diagrams," *IEEE J. Electromagn., RF, Microw. Med. Biol.*, vol. 6, no. 3, pp. 429-436, Sep. 2022.
[26] J. H. Chowdhury et al., "Separation of heartbeat waveforms of simultaneous two-subjects using independent component analysis and empirical mode decomposition," *IEEE Microw. Wireless Tech. Lett.*, vol. 34, no. 8, pp. 1059-1062, Aug. 2024.
[27] Z. Liang, M. Xiong, J. Chen, D. Zhao, D. Yang, B. Liang, and J. Mo, "A combined algorithm for non-contact human vital signs monitoring using IR-UWB radar," in *Proc. Int. Conf. Microw. Millim. Wave Technol. (ICMMT)*, Qingdao, China, May 2023, pp. 1-3.
[28] K. Dragomiretskiy and D. Zosso, "Variational mode decomposition," *IEEE Trans. Signal Process.*, vol. 62, no. 3, pp. 531–544, Feb. 2013.
[29] P. Chen, Y. Du, W. Huang, Y. Bai, S. Wei, and J. Wang, "Vehicle occupant detection and vital sign monitoring based on random body movement correction using millimeter-wave radar," *IEEE Sens. J.*, vol. 25, no. 12, pp. 21945–21957, Jun. 2025.
[30] L. Liu, J. Zhang, Y. Qu, S. Zhang, and W. Xiao, "MmRH: Noncontact vital sign detection with an FMCW mm-wave radar," *IEEE Sens. J.*, vol. 23, no. 8, pp. 8856–8866, Apr. 2023.
[31] J.-Y. Kim, J.-H. Park, S.-Y. Jang, and J.-R. Yang, "Peak detection algorithm for vital sign detection using Doppler radar sensors," *Sensors*, vol. 19, no. 7, Art. no. 1575, Apr. 2019.
[32] Z. Liu, Y. Xiong, W. Tian, Y. Gou, and Z. Peng, "Large-scale body movement cancellation in FMCW radar respiration detection," *IEEE Trans. Microw. Theory Techn.*, vol. 73, no. 5, pp. 2992-3003, May 2025.
[33] C. Ni, J. Pan, D. Du, X. Yang, C. Shi, S. Chen, D. Yang, and S. Liu, "Accurate heart rate measurement across various body postures using FMCW radar," *IEEE Trans. Instrum. Meas.*, vol. 73, pp. 1–13, 2024.
[34] D. Xu, W. Yu, Y. Wang, and M. Chen, "Vital signs detection in the presence of nonperiodic body movements," *IEEE Trans. Instrum. Meas.*, vol. 73, pp. 1–16, 2024.
[35] X. Qiao, Y. Su, X. Li, and T. Shan, "Millimeter-wave radar vital signs measurement with random body movement using missing data model," *IEEE Trans. Instrum. Meas.*, vol. 74, pp. 1–14, 2025.
[36] W. Li, Y. Xiong, S. Hong, Z. Liu, and Z. Peng, "Wide range and accurate displacement measurement technique using FMCW radar," *IEEE Microw. Wireless Tech. Lett.*, vol. 35, no. 4, pp. 492–495, Apr. 2025.
[37] S. Yoon, S. Ahmed, S. Abdullah, and S. H. Cho, "Remote vital sign monitoring with IMU assisted handheld IR-UWB radar sensor," *IEEE Sens. J.*, vol. 25, no. 16, pp. 31910-31921, Aug. 2025.
[38] G. Mauro, M. De Carlos Diez, J. Ott, L. Servadei, M. P. Cuellar, and D. P. Morales-Santos, "Few-shot user-adaptable radar-based breath signal sensing," *Sensors*, vol. 23, no. 2, Art. no. 804, Jan. 2023.
[39] H. Wang, "HeRe: Heartbeat signal reconstruction for low-power millimeter-wave radar based on deep learning," *IEEE Trans. Instrum. Meas.*, vol. 72, pp. 1–15, 2023.
[40] P. E. Numan, H. Park, J. Lee, and S. Kim, "Machine learning-based joint vital signs and occupancy detection with IR-UWB sensor," *IEEE Sens. J.*, vol. 23, no. 7, pp. 7475–7482, Apr. 2023.
[41] L. Qu, C. Liu, T. Yang, and Y. Sun, "Vital sign detection of FMCW radar based on improved adaptive parameter variational mode decomposition," *IEEE Sens. J.*, vol. 23, no. 20, pp. 25048–25060, Oct. 2023.

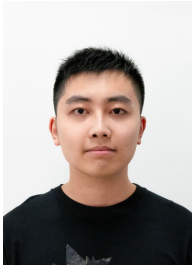

Shihao Zhang received his B.S. degree majoring in measurement and control technology and instrument from Hebei University of Technology, Tianjin, China, in 2023. He is pursuing his MSc degree majoring in instrumentation and meter engineering at Hebei University of Technology, Tianjin, China. His research interests include millimeter-wave radar sensing technique, human vital signs detection and health analysis, and integrated sensing and communication (ISAC) for search and rescue.

Zhaozong Meng (Member, IEEE) received his B.S. degree from Sichuan University, Chengdu, China, in 2006, his M.S. degree from Beihang University, Beijing, China, in 2009, and his Ph.D. degree from the University of Huddersfield, West Yorkshire, U.K., in 2014. He worked as a research associate with the University of Manchester, U.K., from 2014 to 2016, and as a research fellow with the University of Southampton, U.K., from 2016 to 2018. He is now a professor at Hebei University of Technology, Tianjin, China. His research interests include novel sensing techniques, wearable devices and body area networks, and cyber-physical systems.

Yongwei Zhang (Member, IEEE) received the B.S. degree in communication engineering from Jilin University, Changchun, China, in 1996, and the Ph.D. degree from the School of Electrical and Electronic Engineering, The University of Manchester, Manchester, U.K., in 2007. In 1996, he joined Lucent Technologies (AT&T initially), Qingdao, China, where he was first an Application Engineer on the 5ESS system and later a System Engineer, and had worked there until 2003. While he was working at Lucent Technologies, in 1998, he was sent as a Visitor to Bell Laboratories, Naperville, IL, USA, trained in communication system engineering tool development, and later certified as an international instructor. In the years working for Lucent Technologies from 1996 to 2003, he was involved in 5ESS switch application engineering and optimization for wireless communication systems. In 2003, he joined The University of Manchester, Manchester, U.K., as a Ph.D. candidate, a Research Fellow, and the Task Leader of the front-end design work package in the Mid-Frequency Aperture Array Consortium for the Square Kilometre Array (SKA). His current research interests include antenna design based on flexible materials, electromagnetic theories, antenna array design and calibration, and radio astronomy instrumentation. Dr. Zhang was awarded as an Outstanding Member of the PHS Project Team in 2000 and received the 2001 Chairman Award from Lucent Technologies (China) Company Ltd.

MURAT TEMİZ (Member, IEEE) received the B.S. degree from Gazi University, Ankara, Turkey, in 2011, the M.S. degree from the TOBB University of Economics and Technology, Ankara, in 2013, and the Ph.D. degree from the Department of Electrical and Electronic Engineering, The University of Manchester, Manchester, U.K., in 2020. He is also working as a Research Assistant focusing on massive multiple-input–multiple-output (MIMO) communication, MIMO orthogonal frequency-division multiplexing (OFDM) radars, and high energy efficiency integrated radar and communication systems at the Department of Electrical and Electronic Engineering, The University of Manchester. His current research interests include massive MIMO systems, antenna array design, channel measurements, optimization, integrated sensing and communications, and machine learning applications.

ORHAN KAPLAN (Member, IEEE) was born in Erzincan, Türkiye, in 1978. He received the B.Sc. degree from Gazi University, Ankara, Türkiye, in 2001, and the M.Sc. and Ph.D. degrees in electrical education from the Institute of Science and Technology, Gazi University, Ankara, in 2005 and 2011, respectively. He is currently an Associate Professor with the Faculty of Technology, Department of Electrical and Electronics Engineering, Gazi University. His current research interests include nonlinear control, electrical machines, and power electronic converters.

Nan Gao received his B.S., M.S., and Ph.D. degrees in biomedical engineering from Tianjin University, Tianjin, China, in 2006, 2008, and 2012, respectively. Since 2012, he has been a Lecturer with the School of Mechanical Engineering, Hebei University of Technology, Tianjin, where he has been promoted an Associate Professor in 2019. His research interests include spectral analysis, computer vision, 3D precision measurement, and image processing.

Zonghua Zhang received his B.S., M.S., and Ph.D. degrees from Tianjin University, Tianjin, China, in 1996, 1998, and 2001, respectively. From 2002 to 2009, he was a Research Fellow with Hong Kong Polytechnic University, Ruhr-Universität Bochum, Queen's University, Heriot-Watt University, and the University of Leeds. From 2016 to 2018, he was awarded the EU "Marie Curie Individual Fellowship" and worked with the University of Huddersfield. Since 2009, he has been a Professor at Hebei University of Technology. His research interests include optical 3D precision measurement, phase calculation-based 3D measurement, and phase measuring deflectometry.